Potential energy surfaces and bound states for the open-shell van der Waals cluster Br–HF

Markus Meuwly and Jeremy M. Hutson

Citation: The Journal of Chemical Physics **119**, 8873 (2003); doi: 10.1063/1.1615238
View online: http://dx.doi.org/10.1063/1.1615238
View Table of Contents: http://scitation.aip.org/content/aip/journal/jcp/119/17?ver=pdfcov
Published by the AIP Publishing

Potential energy surfaces and bound states for the open-shell van der Waals cluster Br–HF

Markus Meuwly[a)]
Department of Chemistry, University of Basel, Klingelbergstrasse 80, 4056 Basel, Switzerland

Jeremy M. Hutson[b)]
Department of Chemistry, University of Durham, South Road, Durham, DH1 3LE, United Kingdom

(Received 26 June 2003; accepted 11 August 2003)

Semiempirical potential energy surfaces for the lowest three electronic states of the open-shell complex Br–HF are constructed, based on existing empirical potentials for Kr–HF and Kr–Ne and coupled-cluster electronic structure calculations for Br–Ne. Coupled cluster calculations are also described for He–F, Ne–F and Ar–F. Electrostatic interactions that arise from the quadrupole of the Br atom and the permanent multipoles of HF are also included in the Br–HF surfaces. The well depth of the lowest adiabatic surface is found to be 670 cm^{-1} at a linear equilibrium geometry. The results of helicity decoupled and full close-coupling calculations of the bound states of the complex are also described. The ground state, with total angular momentum projection quantum number $|P|=3/2$, is found 435 cm^{-1} below dissociation to $Br(^2P_{3/2})+HF(j=0)$. The lowest-frequency intermolecular bending and stretching vibrations are predicted around 145 and 211 cm^{-1}, respectively. Parity splittings are found to be extremely small for bound states with projection quantum number $|P|=3/2$. The relevance of the results to recently recorded spectra of Br–HF is discussed. © *2003 American Institute of Physics.* [DOI: 10.1063/1.1615238]

I. INTRODUCTION

Molecular complexes involving open-shell constituents are attracting increasing interest, both experimental and theoretical, because their spectra can provide detailed information on potential energy surfaces in the entrance and exit valleys of chemical reactions. Complexes formed between halogen atoms and hydrogen halides are particularly interesting, because their spectra would probe the potential energy surfaces for prototype hydrogen exchange reactions such as Cl+HCl and F+HF. In 1994, Dubernet and Hutson[1] pointed out that, for atom-diatom systems containing atoms in *P* states, there would be a substantial long-range well arising from the electrostatic interaction of the atomic quadrupole moment with the permanent multipole moments of the diatom. For Cl–HCl, they developed a model potential[2] based on combining the known Ar–HCl and Ar–Cl potentials with electrostatic dipole–quadrupole and quadrupole–quadrupole terms. The model gave surfaces for the three lowest electronic states of Cl–HCl (correlating with $Cl\,^2P_{3/2}$ and $^2P_{1/2}$), with a well depth of 383 cm^{-1} for the lowest adiabatic surface at a linear Cl–H–Cl geometry and a plateau at a T-shaped geometry. The well depth for Cl–HCl may be compared with that for the nearly isoelectronic system Ar–HCl,[3] which is only 176 cm^{-1}. The difference arises principally from the electrostatic terms, which are absent in Ar–HCl. Dubernet and Hutson[2] used these surfaces to carry out fully nonadiabatic calculations of the bound states of the Cl–HCl complex, including all three surfaces and spin–orbit coupling effects. More recently, Meuwly and Hutson have carried out analogous calculations for F–HF[4] and Br–HBr,[5] for which the model gave well depths of 317 and 342 cm^{-1}, respectively.

The large electrostatic wells in systems containing *P*-state atoms have important consequences for reactive scattering. For example, Maierle *et al.*[6] and Dobbyn *et al.*[7] have developed full reactive potentials for Cl–HCl that incorporate the Dubernet–Hutson potential at long range, and these have been used to show that the long-range well has important effects on the positions of reactive scattering resonances and to calculate thermal rate coefficients.[8,9] Xie *et al.*[10] have shown that long-range forces are responsible for prominent resonances in the $O(^3P)+HCl$ reaction, while Skouteris *et al.*[11] have shown that such forces play a decisive role in determining the product isotope ratio in the Cl+HD reaction.

In recent work, Kłos *et al.*[12] and Ždánska *et al.*[13] have obtained fully *ab initio* potential energy surfaces for the three lowest electronic states of Cl–HCl. Both groups obtained surfaces in qualitative agreement with the semiempirical surfaces of Dubernet and Hutson.[1] Those of Ždánska *et al.*, who used the multireference coupled pair functional (MRACPF) method, are also in reasonable quantitative agreement with the semiempirical results, though their linear well is slightly shallower and the T-shaped plateau has moved inwards and become a secondary minimum. Kłos *et al.*, who used coupled cluster calculations, did not explicitly describe surfaces including spin–orbit coupling, but their lowest spin-free surface is about 14% deeper than the corresponding Dubernet–Hutson surface at the linear geometry and has a well 600 cm^{-1} deep (now the absolute minimum) at a T-shaped structure. This well will be at least partially washed

a)Electronic mail: m.meuwly@unibas.ch
b)Electronic mail: j.m.hutson@durham.ac.uk

out when spin–orbit coupling is introduced, but may be deep enough to remain the primary minimum.

Complexes such as Cl–HCl and Br–HBr are attractive candidates for experimental spectroscopy. They are ''prereactive'' species (entrance channel complexes), in which absorption of a photon might stimulate a chemical reaction starting from a well-defined initial state. Wittig and co-workers[14,15] have attributed structure in the H atom kinetic energy distributions resulting from photodissociation of HCl in HCl dimer to the formation of a Cl–HCl product. The Cl–HCl and Cl–DCl products have been further studied by Imura *et al.*[16] and Che *et al.*[17] There have also been attempts to make Cl–HCl complexes directly in molecular beams and jets, but these have not yet to our knowledge been successful. However, Miller and co-workers[18] have recently succeeded in forming the related complex Br–HF in liquid helium droplets and have observed the infrared spectrum of the HF stretching band in the complex. The purpose of the present paper is to carry out calculations of the potential energy surfaces and rovibronic levels of Br–HF, in order to assist in interpretation of the new spectra and to suggest additional experiments that might give information on intermolecular bending and stretching modes. Such information would be immensely valuable in learning about the angular and radial shape of the electrostatic potential well.

II. THEORETICAL METHODS

The present work uses a Jacobi coordinate system, in which r is the F–H distance, R is the distance from the HF center of mass to the Br atom and θ is the angle between the vectors corresponding to r and R, measured at the HF center of mass (with $\theta=0$ corresponding to the linear Br–H–F geometry). Vibrations of the HF monomer are not treated explicitly, and the potentials obtained here should be considered to be averages over the vibrational motion of HF.

Open-shell complexes are more complicated than closed-shell complexes, because there are additional angular momenta due to electronic orbital motion and spin. The quantum numbers needed to describe complexes containing open-shell atoms have been discussed by Dubernet and Hutson.[1] As is customary for van der Waals complexes, lower-case letters are used for quantities that refer to the monomers and upper-case letters for those that refer to the complex as a whole. The total orbital and spin quantum numbers of the Br atom are denoted l and s, with resultant j_a and projection ω onto the intermolecular axis. The rotational angular momentum of the HF monomer is denoted j and its rotational constant is b. The total angular momentum of the complex (neglecting nuclear spin) is denoted J and the corresponding rotational constant is B.

The interaction between an atom in a P state and a diatomic molecule can be described in terms of three diabatic or adiabatic (Born–Oppenheimer) surfaces in various ways.[2] The dynamics involve all three surfaces and the couplings between them. Because of this, the surfaces themselves are not enough to understand the dynamics: additional information on the electronic wave functions is required to calculate the coupling matrix elements.

The adiabatic surfaces are useful conceptually and for visualization purposes. For dynamics calculations, however, it is generally more convenient to use a diabatic rather than an adiabatic representation. To a first approximation, the intermolecular interaction is too weak to mix in excited atomic orbitals of the halogen atom, and the atomic orbital angular momentum l (equal to 1 here) is nearly conserved. In the absence of spin–orbit coupling, the three diabatic surfaces are those for interaction of HF with a Br atom with its unpaired electron in a pure p_x, p_y or p_z orbital (with the z axis along the intermolecular vector R and the three atoms lying in the xz plane). An alternative way to view this is to introduce angles θ_a and ϕ_a that are conjugate to l and m_l: in a simple picture, θ_a and ϕ_a may be thought of as the angular coordinates of the hole in the incomplete p shell. The resulting potential depends on the intermolecular distance R and three angles, θ, θ_a, and ϕ_a, and thus bears similarities to a diatom–diatom interaction potential.

A. Model potential for Br–HF

We have constructed a model intermolecular potential for Br–HF using the procedure previously employed for the symmetric open-shell complexes Cl–HCl, F–HF, and Br–HBr.[2,4,5] In this model the potential anisotropy for Br–HF is taken from the near-isoelectronic Kr–HF and Br–Ne potentials, and supplemented with long-range electrostatic forces involving the Br quadrupole and the permanent multipole moments of HF. The potential for Br–HF is written

$$V_{\mathrm{Br-HF}}(R,\theta,\theta_a,\phi_a)=V_{\mathrm{Kr-HF}}(R,\theta)+V_{\mathrm{Br-Ne}}(R,\theta_a)-V_{\mathrm{Kr-Ne}}(R)+V_{\mathrm{Q}}(R,\theta,\theta_a,\phi_a). \tag{1}$$

The first anisotropic term comes from the anisotropy of the HF molecule, and is modeled in terms of the Kr–HF potential. The Kr–HF surface used in the present work is an old one obtained principally by fitting to microwave spectra of the Kr–HF van der Waals complex;[19] it is qualitatively reasonable, but not of accuracy comparable to those for Ar–HCl[3] and Ne–HF[20] used in our work on Cl–HCl[2] and F–HF,[4] which were fitted to much more extensive spectroscopic information.

The second anisotropic contribution comes from the anisotropy of the Br atom, and is modeled in terms of the potential curves for the Br–Ne interaction. Atomic Br has a ^2P ground state with the configuration $[\mathrm{Ar}](3d)^{10}(4s)^2(4p)^5$. Upon complexation with Ne, the unpaired electron of Br may occupy a p_x, p_y or p_z orbital (configurations $p_x^1p_y^2p_z^2$, $p_x^2p_y^1p_z^2$, and $p_x^2p_y^2p_z^1$). Since the z axis is the interatomic axis, the first two of these are degenerate and form a Π state with potential curve $V_\Pi(R)$, while the third forms a Σ state with potential curve $V_\Sigma(R)$. For halogen atom–rare gas interactions, the Σ curve is in general deeper than the Π curve because the rare gas atom can approach closer along the axis of the partially filled p orbital than perpendicular to it. The isotropic and anisotropic components $V_0(R)$ and $V_2(R)$ are related to $V_\Sigma(R)$ and $V_\Pi(R)$ by[21,22]

TABLE I. Well depths and equilibrium distances for Rg–F and Ne–Br potentials from scattering experiments (Ref. 21) and theory (this work).

	He–F		Ne–F		Ar–F		Ne–Br
	Expt.	Theory	Expt.	Theory	Expt.	Theory	theory
Σ state ($\Lambda=0$)							
D_e/cm^{-1}	−18.5	−24.4	−61.3	−41.6	−96.8	−94.8	−53.1
R_e/Å	3.00	2.84	2.90	2.94	3.12	3.12	3.57
σ/Å	2.67	2.50	2.61	2.61	2.73	2.75	3.18
Π state ($\Lambda=1$)							
D_e/cm^{-1}	−16.9	−10.7	−26.6	−21.7	−46.8	−42.1	−31.8
R_e/Å	3.04	3.28	3.26	3.31	3.61	3.62	3.94
σ/Å	2.72	2.93	2.91	3.00	3.20	3.27	3.53

$$V_0(R)=\tfrac{1}{3}(V_\Sigma(R)+2V_\Pi(R)), \tag{2}$$

$$V_2(R)=\tfrac{5}{3}(V_\Sigma(R)-V_\Pi(R)). \tag{3}$$

The curves used for Br–Ne in the present work are obtained from *ab initio* calculations as described below.

The last term in Eq. (1) is the electrostatic term that arises from the interaction of the atomic quadrupole on Br with the multipoles on HF. This interaction may be approximated by

$$V_\mathrm{Q}(R,\theta,\theta_a,\phi_a)=\frac{\sqrt{15}e\langle r_a^2\rangle\mu_\mathrm{HF}\mathcal{I}_{123}}{R^4}+\frac{\sqrt{70}e\langle r_a^2\rangle\Theta_\mathrm{HF}\mathcal{I}_{224}}{R^5}, \tag{4}$$

where the $\mathcal{I}$ functions are as defined in Eq. (4) of Ref. 1 and $\mu_\mathrm{HF}=0.7069ea_0$ and $\Theta_\mathrm{HF}=1.7337ea_0^2$ are the permanent dipole and quadrupole moments of HF in its $v=0$ state. The quantity $\langle r_a^2\rangle$ is the mean square radius of the incomplete atomic shell of Br, which is related to the permanent atomic quadrupole moment Θ_a by $\Theta_a=\frac{2}{5}e\langle r_a^2\rangle$. The value $\Theta_a=2.196ea_0^2$ from a relativistic CASPT2 calculation on the Br atom[23] was used here. The Kr–Ne potential used in the present work is that of Barrow *et al.*[24]

B. Electronic structure calculations for rare gas–halogen atom systems

For most of the atomic halogen–rare gas systems, empirical potential curves have been obtained by inversion of results from molecular beam scattering experiments.[21,22] However, to the best of our knowledge no such potentials exist for Br–Ne. We have therefore calculated Σ and Π curves for this interaction using *ab initio* electronic structure methods. The calculations were carried out at the RCCSD(T) level (restricted coupled cluster calculations with single, double, and noniterative triple excitations), using aug-cc-pVQZ basis sets.[25,26] All calculations were carried out using the MOLPRO2000 package[27] and were corrected for basis set superposition error using the counterpoise method.[28]

To assess the accuracy of the electronic structure methods used here [RCCSD(T)/aug-cc-pVQZ], the potentials V_Σ and V_Π were also calculated for the family of Rg–F systems with Rg=He, Ne, and Ar. For these species, V_Σ and V_Π and the corresponding isotropic and anisotropic components of the intermolecular interaction have also been obtained from inversion of experimental scattering data.[21] The calculated points were fitted to a series expansion composed of a short-range repulsion and a long-range attraction,

$$V(R)=(a_2+a_3(R-a_0))\exp(-a_1(R-a_0))+\frac{1}{2}(1+\tanh(a_4+a_5(R-a_0)))\times\left(\frac{C_6}{R^6}+\frac{C_8}{R^8}+\frac{C_{10}}{R^{10}}\right). \tag{5}$$

A similar form has been used previously by Kłos *et al.*[31] The C_6 coefficients were fixed at values obtained from a combining rule based on the Slater–Kirkwood formula,[29]

$$C_6^{\mathrm{RgX}}=\frac{3\alpha_\mathrm{Rg}\alpha_\mathrm{X}\eta_\mathrm{Rg}\eta_\mathrm{X}}{2(\eta_\mathrm{Rg}+\eta_\mathrm{X})}, \tag{6}$$

where $\eta=[N_\mathrm{eff}/\alpha]^{1/2}$ and values of the static polarizabilities α and effective number of electrons N_eff for the rare gases were taken from Table I of Ref. 30. The anisotropic polarizabilities of halogen atoms were taken from Medved *et al.*,[23] and the values of N_eff for F and Br were taken to be 3.5 and 6.0, respectively; these values of N_eff are about 0.3 less than those for the near-isoelectronic rare gas atoms.

The resulting equilibrium distances R_e, positions of the repulsive wall σ, and dissociation energies D_e for the Σ and Π state potentials are summarized and compared with the experimental values in Table I. Table II gives the parameters of our fits.

There are some rather large differences between the calculated and empirical potentials for He–F and Ne–F, but the uncertainties in the empirical potential wells are substantial for these systems; they can be up to 30% for well depths and around 5% for the equilibrium bond lengths.[31] The *ab initio* potentials show more consistent trends down the series from He to Ar than the empirical ones: the minimum in $V_\Sigma(R)$ is always 0.35 to 0.5 Å inside that in $V_\Pi(R)$ and the well depth for the Σ curve is a factor of 1.8 to 2.3 larger. For the empirical potentials the distance shift ranges from 0.04 to 0.45 Å and the well depth factor ranges from 1.09 to 2.30.

TABLE II. Parameters describing the RCCSD(T)/aug-cc-pVQZ Rg–F and Ne–Br potentials.

	State	a_0 Å	a_1 Å^{-1}	a_2 cm^{-1}	a_3 cm^{-1} Å^{-1}	a_4	a_5 Å^{-1}	C_6 cm^{-1} Å^6	C_8 cm^{-1} Å^8	C_{10} cm^{-1} Å^{10}
He–F	Σ	3.066	1.883	−63.865	1.013	0.922	0.777	1.73*e*+4	9.4*e*+4	1.2*e*+6
	Π	2.477	1.436	−48.518	0.304	0.071	−1.373	1.90*e*+4	1.7*e*+5	1.8*e*+6
Ne–F	Σ	2.547	1.577	−107.894	0.032	−0.228	−1.737	3.62*e*+4	2.3*e*+5	1.0*e*+6
	Π	2.500	1.300	−74.680	−1.230	0.957	−2.700	4.00*e*+4	2.9*e*+5	1.4*e*+6
Ar–F	Σ	3.020	1.481	−155.680	−0.288	−0.613	−1.591	1.13*e*+5	8.0*e*+5	1.5*e*+6
	Π	3.100	1.190	−92.470	−1.500	0.196	−2.597	1.26*e*+5	9.9*e*+5	3.0*e*+6
Ne–Br	Σ	3.333	1.302	−99.180	0.333	−0.534	−1.548	1.40*e*+5	1.0*e*+6	1.1*e*+7
	Π	3.237	1.179	−99.970	0.942	−0.047	−1.403	1.56*e*+5	2.0*e*+6	2.5*e*+7

The empirical potential energy curves suggest that the equilibrium distance for the Σ state actually *shortens* by about 0.1 Å in going from He to Ne.

For Ne–F, where the differences between the calculated and empirical curves are largest, additional calculations at the RCCSD(T)/aug-cc-pV5Z level were carried out. As expected, the dissociation energies increased slightly (by 5%–10%) and the equilibrium distances decreased slightly (by 0.01–0.03 Å). The aug-cc-pV5Z results on the Σ state give $D_e = 45.0\,\mathrm{cm}^{-1}$ at $R_e = 2.93$ Å and on the Π state give $D_e = 24.0\,\mathrm{cm}^{-1}$ at $R_e = 3.28$ Å. However, the change in the Σ state well depth is small compared to the discrepancy with the empirical value (61.3 cm^{-1}). On the whole, it seems likely that the calculated potential curves are more reliable than the empirical ones, although it would probably be possible to improve them by morphing them[32] to fit the experimental data. The fractional change between the aug-cc-pVQZ and aug-cc-pV5Z basis sets for Ne–F probably places an upper limit on the errors in the calculations for He–F and Ar–F: correlated calculations with Ne atoms are notoriously difficult.

From these comparisons it appears that calculations at the RCCSD(T)/aug-cc-pVQZ level provide a good compromise between accuracy and computational expense for calculating the potential energy curves for Br–Ne needed in the model. The calculated $V_\Sigma(R)$, $V_\Pi(R)$ and the derived curves $V_0(R)$ and $V_2(R)$ for Br–Ne are shown in Fig. 1 together with the *ab initio* calculated energies. The Σ potential has a well depth of 53.1 cm^{-1} at 3.57 Å and the Π curve has $D_e = 31.8\,\mathrm{cm}^{-1}$ at $R_e = 3.94$ Å.

C. Potential energy surfaces neglecting spin

The different representations that can be used for the potential energy surfaces for X–HX systems have been discussed in Ref. 2. This section will therefore concentrate on the results for Br–HF and a comparison with the previous results on Cl–HCl,[2] Br–HBr,[5] and F–HF.[4]

Figure 2 shows the diabatic and adiabatic surfaces in the spin-free representation (neglecting spin–orbit coupling). The spin–orbit coupling in the Br atom is in fact so large that the diagonal diabatic surfaces by themselves are not particularly useful in visualizing the results of dynamical calculations. Nevertheless, the spin-free diabatic *representation* (with both diagonal and off-diagonal parts, and supplemented with spin–orbit coupling information) is the one that is used in the dynamical calculations and is fairly readily extracted from *ab initio* calculations.[12] The spin-free adiabatic surfaces are also important because they are the ones that would result directly from an *ab initio* calculation excluding spin–orbit coupling.

The spin-free diabatic potentials are the diagonal elements of the Hamiltonian in a basis set of atomic functions quantized along the *x*, *y*, and *z* axes. The p_x and p_y diabats are degenerate for $\theta = 0$ and 180° but diverge as the geometry departs from linear (a Renner–Teller effect). They both have a deep well at $\theta = 0$. Their absolute well depth is 670 cm^{-1}. This is about twice the depth found for either F–HF or Br–HBr; it arises because the Br atom has a larger quadrupole moment than F, while HF has a larger dipole moment and can approach closer than HBr. The secondary minimum (at

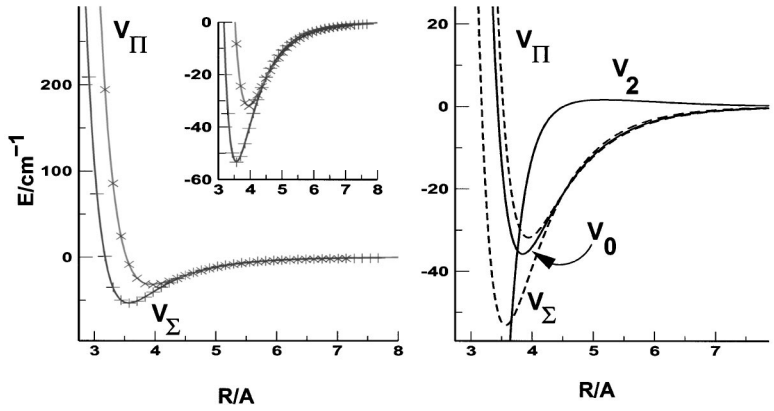

FIG. 1. Left panel: potential curves for the spin-free Σ and Π states of Br–HF, calculated at the RCCSD(T)/aug-cc-pVQZ level together with the *ab initio* points. Right panel: potential curves for the isotropic $V_0(R)$ and anisotropic $V_2(R)$ components (solid lines) of the Br–Ne interaction.

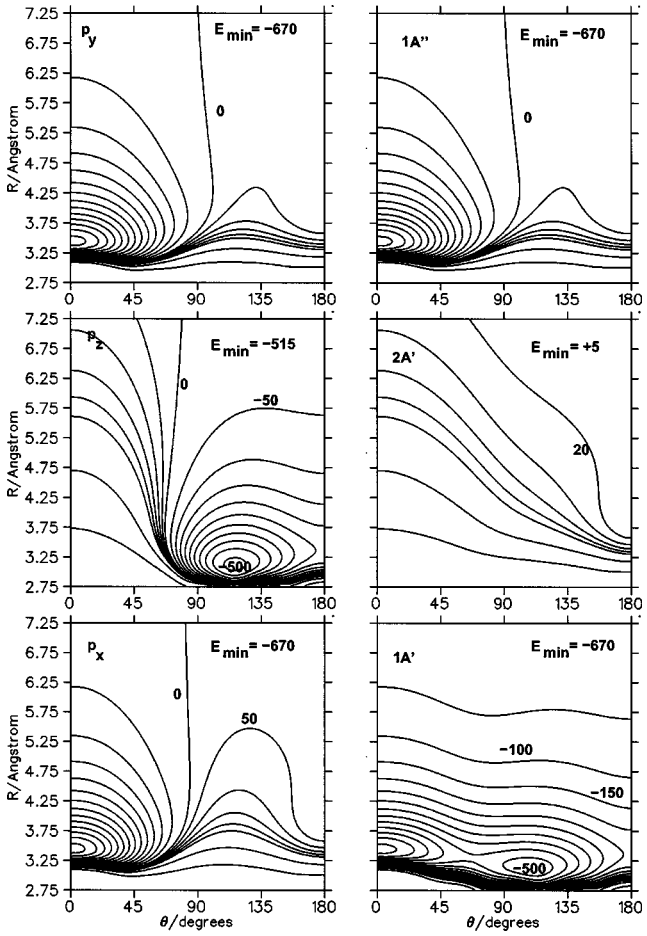

FIG. 2. Contour plots of the Br–HF interaction potentials excluding spin. Diabatic surfaces are shown on the left and adiabatic surfaces ($1A'$, $2A'$, $1A''$ from bottom to top) on the right. Contours are drawn every 50 cm^{-1} up to 0 cm^{-1}, every 20 cm^{-1} up to 100 cm^{-1}, and at 200 and 500 cm^{-1}.

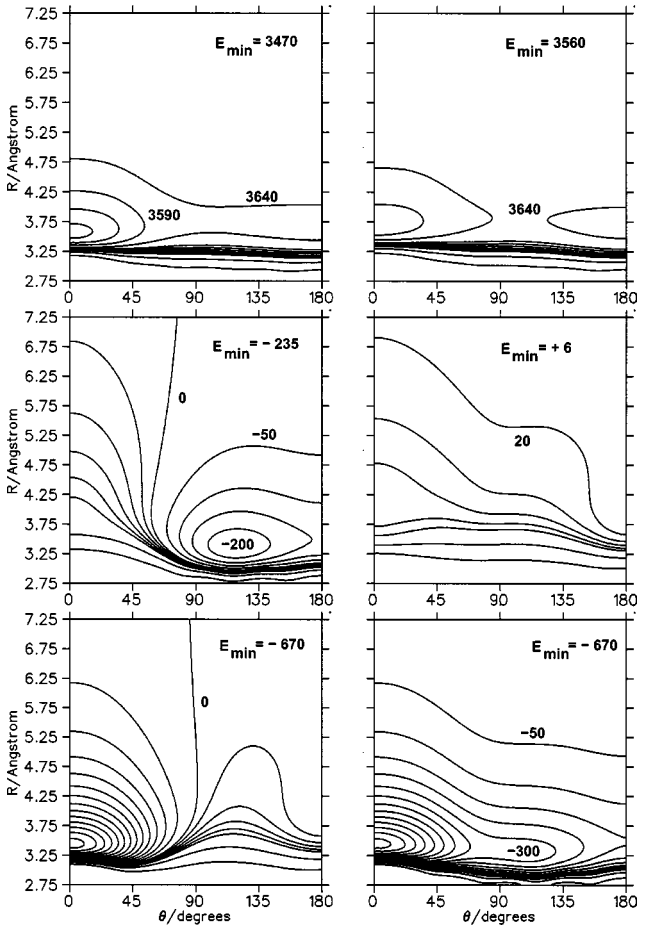

FIG. 3. Contour plots of the Br–HF interaction potentials including spin. Diabatic surfaces [$(j_a,|\omega|)=(3/2,3/2)$, $(3/2,1/2)$, $(1/2,1/2)$ from bottom to top] are shown on the left and adiabatic surfaces on the right. In each case the lower two plots show the surfaces correlating with Br ($^2P_{3/2}$) and the top plot shows the surface correlating with Br ($^2P_{1/2}$). Contours are drawn every 50 cm^{-1} up to 0 cm^{-1}, every 20 cm^{-1} up to 100 cm^{-1}, and at 200 and 500 cm^{-1}.

+6 cm^{-1}, not visible in Fig. 2), at the Br–FH geometry, has a very much shallower well than the primary minimum because of unfavorable quadrupole–dipole interactions.

The minimum-energy structure on the p_z diabat is close to $\theta=120°$. This can again be explained by purely electrostatic considerations: this is the geometry that optimizes the interaction of the HF dipole and quadrupole when the Br atomic quadrupole is oriented along the *z* axis.

The spin-free potential energy surfaces can be expressed in an adiabatic form by diagonalizing the matrix representation of the potential in the basis set of atomic functions. The transformation leaves the p_y surface unchanged but mixes the p_x and p_z potentials through the off-diagonal elements described in Ref. 2. The diagonalization produces two surfaces of A' symmetry and one of A'' symmetry (corresponding to unmixed p_y). The minimum of the lowest adiabat ($1A'$) is at a linear configuration with a well depth of 670 cm^{-1}. This is qualitatively different from Cl–HCl and F–HF, where there were both linear and T-shaped minima but the linear minimum was slightly deeper, and for Br–HBr, where the T-shaped minimum was deeper. The upper A' adiabat ($2A'$) has only a very shallow minimum, 5 cm^{-1} deep at the linear Br–FH geometry, and is repulsive over most of the angular range. The *ab initio* results for Cl–HCl[12,13] suggest that the semiempirical potential in that case is insufficiently attractive at the T-shaped geometry. However, this may well be less of a problem for Br–HF, because Br is considerably less electronegative than F and incipient chemical bonding is likely to be less significant.

D. Potential energy surfaces including spin–orbit coupling

The spin–orbit coupling in the Br atom can either be regarded as coupling the spin-free states, or it can be included in the description of the potential surfaces. In Br–HBr, the spin–orbit coupling is so large that the latter is physically more sensible for visualization purposes. To construct surfaces that include spin–orbit coupling, we assume that the coupling in the complex is the same as in the isolated Br atom, and is of the form $\xi\hat{\mathbf{l}}\cdot\hat{\mathbf{s}}$, where $\xi=-2457$ cm^{-1}. The matrix representation is constructed in a basis set of atomic orbital functions for $l=1$ and spin functions for $s=1/2$, with resultant $j_a=1/2$ or $3/2$ and projection ω onto the intermolecular axis. The resulting 6×6 matrix has three pairs of equal diagonal elements and three doubly degenerate pairs of

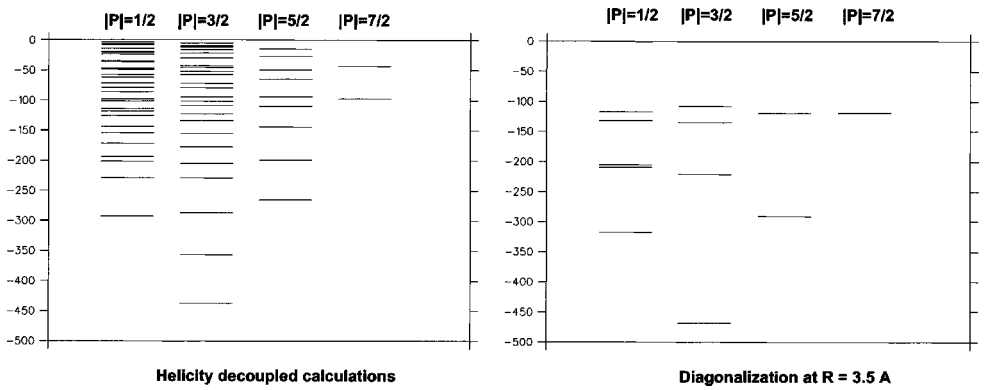

FIG. 4. Pattern of all levels in the helicity decoupled approximation (left), compared with the bending levels calculated by diagonalizing the helicity decoupling matrix at $R=3.5$ Å (right).

eigenvalues; either the diagonal elements (diabats) or the eigenvalues (adiabats) can be plotted. Contour plots of the resulting surfaces are shown in Fig. 3.

Two diabatic surfaces correspond to $j_a=3/2$ with $|\omega|=3/2$ and 1/2 and one to $j_a=1/2$ with $|\omega|=1/2$. The last is shifted upwards at long range by the atomic spin–orbit splitting, $\frac{3}{2}|\xi|$. The two $j_a=3/2$ diabats are qualitatively (but not quantitatively) similar to the p_x and p_z diabats. As for the symmetric systems, however, the $j_a=1/2$, $|\omega|=1/2$ diabat is quite different from any of the spin-free diabats. This is because an atomic state with $j_a<1$ cannot have an overall quadrupole moment. The attractive electrostatic components thus make no contribution to the $j_a=1/2$ diabat, and its anisotropy stems solely from that of the Kr–HF potential.

The right-hand side of Fig. 3 shows the adiabatic surfaces obtained when spin–orbit coupling is included. There are again two surfaces that correlate at long range with Br$(^2P_{3/2})$ and one that correlates with Br$(^2P_{1/2})$. On the lowest adiabat, Br–HF has a single linear minimum 670 cm^{-1} deep and a very shallow secondary minimum with a depth of 275 cm^{-1} between $\theta=90°$ and 130°. This is fairly similar to Cl–HCl, though without a secondary minimum at $\theta=180°$.

The second adiabat for Br–HF also correlates with Br$(^2P_{3/2})$ and is qualitatively similar to the second spin-free adiabat, with a minimum 6 cm^{-1} deep at the Br–FH structure. The highest-lying adiabat, which correlates with Br$(^2P_{1/2})$, is qualitatively similar to its diabatic $j_a=1/2$, $|\omega|=1/2$ counterpart, because the large spin–orbit splitting in Br prevents strong mixing of $j_a=1/2$ and 3/2.

III. BOUND-STATE CALCULATIONS

We have used the BOUND program[33] to carry out helicity decoupled and close-coupling calculations of the bound vibrational-rotation states supported by the model potential for Br–HF. The methods used have been described in detail in Ref. 2; they include all three surfaces and the couplings between them, as well as spin–orbit coupling. The total wave function is expanded using rigid rotor functions for HF and coupled angular momentum basis functions for the complex as a whole. The HF molecule is treated as a rigid rotor with a rotational constant $b=20.559\,743$ cm^{-1}, appropriate for the $v=0$ state of HF. The basis set includes all monomer functions up to $j=15$.

A. Helicity decoupling calculations

In the helicity decoupling approximation,[2] the basis functions are labeled by P, the projection of the total angular momentum J onto the intermolecular axis, and terms off-diagonal in P are neglected. Such calculations give no information about parity splittings, and the rotational constants derived from them are approximate. Nevertheless, they provide a useful starting point for investigating the level patterns.

It is useful first to consider the pattern of bending levels, uncomplicated by the intermolecular stretch. The right-hand side of Fig. 4 shows the pattern of bending levels, obtained by diagonalizing the helicity decoupled matrix at a fixed intermolecular distance, $R=3.5$ Å. The lowest level has $|P|=3/2$. It can essentially be regarded as a bending state of a linear molecule with bending quantum number $v_b=0$, vibrational angular momentum $k=0$ and $|\omega|=3/2$. For Br–HF this state is bound by 471 cm^{-1}. The next two bending states correspond to HF internal rotation states with vibrational angular momentum $k=\pm1$ and hence $|P|=1/2$ and 5/2, bound by 319 and 293 cm^{-1}, respectively.

The next level of approximation is to solve coupled differential equations by propagating in R, rather than simply diagonalize the bending Hamiltonian at a fixed value of R. The resulting coupled equations are solved numerically using a log-derivative propagator.[34] The methods used to solve the coupled equations are described in detail in Ref. 35. The Br–HF reduced mass is taken to be $15.960\,221m_u$ [where $m_u=m_a(^{12}\mathrm{C})/12$]. The coupled equations are propagated from $R_{\min}=2.5$ Å to $R_{\max}=8$ Å, extrapolating to zero step size from log-derivative interval sizes of 0.025 and 0.05 Å using Richardson h^4 extrapolation. Increasing the propagation range or decreasing the step size changes the eigenvalues by less than 10^{-4} cm^{-1}.

Coupled channel helicity decoupling calculations were carried out for values of $|P|$ ranging from 1/2 to 7/2. The resulting energy levels are collected in Table III. No bound states with $|P|>7/2$ were found below the lowest dissocia-

TABLE III. Energy levels (above) and spectroscopic parameters (below) from helicity decoupled calculations for Br–HF. All quantities are given in cm^{-1}, with energy levels relative to the energy of $Br(^2P_{3/2})+HF(j=0)$. Derived spectroscopic parameters (in cm^{-1} for *E*, *B*, *D*). Note that more significant figures than are given for the eigenvalues were used in the fits to obtain these values.

n	*P*	*J*=1/2	*J*=3/2	*J*=5/2	*J*=7/2
0	1/2	−290.446	−290.180	−289.736	−289.115
1	1/2	−224.595	−224.338	−223.911	−223.314
0,1	1/2	−197.978	−197.704	−197.248	−196.609
0,1	1/2	−190.020	−189.747	−189.291	−188.652
0	3/2		−435.295	−434.854	−434.236
1	3/2		−353.101	−352.680	−352.090
2	3/2		−282.874	−282.473	−281.911
3	3/2		−224.092	−223.706	−223.166
0	5/2			−262.635	−262.017
1	5/2			−195.171	−194.582

n	$\|P\|$	$E-E_0$	*B*	*D*	$\langle R\rangle$ (Å)	$\langle P_1\rangle$	$\langle P_2\rangle$
0	1/2	144.937	0.0887	5.9×10^{-7}	3.46	0.664	0.271
1	1/2	210.790	0.0854	1.3×10^{-6}	3.54	0.585	0.193
0,1	1/2	237.403	0.0913	8.5×10^{-7}	3.41	−0.217	−0.009
0,1	1/2	245.361	0.0913	1.1×10^{-6}	3.41	0.105	−0.183
0	3/2		0.0882	3.7×10^{-7}	3.46	0.875	0.673
1	3/2	82.200	0.0842	4.9×10^{-7}	3.56	0.863	0.647
2	3/2	152.433	0.0802	6.8×10^{-7}	3.66	0.846	0.613
3	3/2	211.219	0.0772	1.6×10^{-6}	3.65	0.798	0.539
0	5/2	172.224	0.0883	5.6×10^{-7}	3.46	0.709	0.325
1	5/2	239.709	0.0842	7.8×10^{-7}	3.56	0.679	0.277
2	5/2	295.890	0.0805	1.4×10^{-6}	3.46	0.623	0.208
0,1	5/2	329.367	0.0887	1.7×10^{-6}	3.48	0.132	−0.134
0	7/2	339.696	0.0884	8.2×10^{-7}	3.47	0.498	0.001

tion threshold [to $Br(^2P_{3/2})+HF(j=0)$] at 0 cm^{-1}. Excitation of the bending vibration to $v_b=1$, with vibrational angular momentum $k=\pm1$, produces two states with $|P|=1/2$ and 5/2 at vibrational excitation energies of 144.9 cm^{-1} and 172.2 cm^{-1}, respectively. These are the most likely intermolecular vibrations to be observed as infrared combination bands with the HF stretching fundamental. As mentioned above, Kupper *et al.*[18] have observed the HF stretching fundamental of Br–HF at around 3867.4 cm^{-1}, so the present work suggests that combination bands should be sought around 4012 and 4039 cm^{-1}. It would be particularly interesting to locate these experimentally; as we have shown previously for F–HF,[4] the wave functions for these excited states (and especially for the $|P|=1/2$ state) are concentrated on the $|\omega|=1/2$ diabatic surface, and the frequencies would be quite sensitive to any underestimate of the well depth at T-shaped geometries.

To assist with the interpretation of the bound states in the helicity decoupled approximation, rotational constants were calculated for the lower-lying states. They were determined by fitting the energies to the standard energy formula as a function of the total angular momentum *J*,

$$E(J)=E(0)+B(J(J+1)-P^2)-D(J(J+1)-P^2)^2. \qquad (7)$$

The resulting spectroscopic parameters are shown in Table III. From the band energies of the $|P|=3/2$ states and their rotational constants a progression of stretching levels is readily found. The assignment can be verified by comparing the level pattern of the fixed-*R* calculation with the results from the helicity decoupled approximation. For the $|P|=1/2$ and $|P|=5/2$ states the situation is less clear: in both manifolds the first excited state is clearly a stretching state but the higher levels begin to mix and stretch/bend combination states appear.

The calculated ground-state rotational constant ($B=0.0887\,cm^{-1}$) may be compared with that measured in He droplets[18] (0.0450 cm^{-1}). Rotational constants in He droplets are typically reduced compared to gas-phase values, and there is a strong correlation between the droplet:gas-phase ratio and the gas-phase rotational constant itself.[36] The ratio here is 0.51, which is slightly greater than for the comparable complex N_2–HF, where the ratio is 0.42.[36]

It is also of interest to calculate expectation values over radial and angular coordinates. Average intermolecular distances $\langle R\rangle$ and angular expectation values $\langle P_1(\cos\theta)\rangle$ and $\langle P_2(\cos\theta)\rangle$ are reported in Table III. In particular, $\langle P_1(\cos\theta)\rangle$ is related to the dipole moment of the complex. If induced dipoles are neglected, the predicted dipole moment for Br–HF in its ground state is 1.21 D.

B. Close-coupling calculations

Helicity decoupling calculations neglect Coriolis couplings and parity splittings in the energy levels. Such splittings could be measured in microwave spectra or in high-resolution infrared or ultraviolet spectra, so it is worthwhile to investigate them. To do this, we have carried out close-coupling calculations of the lowest few levels, as described in Ref. 2. The close-coupling calculations were performed in the space-fixed representation and produced the energy levels shown in Table IV. We note that in the present calculations the $n=1$, $|P|=1/2$ and $n=3$, $|P|=3/2$ strongly perturb each other for $J>5/2$. Therefore, the spectroscopic constants for the $n=1$, $|P|=1/2$ state were derived from rotational levels $J\leqslant5/2$. In the case of $n=3$, $|P|=3/2$ state only information on the $J=3/2$ and $J=5/2$ levels were used to calculate $E-E_0$ and *B*.

The parity splittings behave differently for $|P|=1/2$ and $|P|=3/2$. For $|P|=1/2$ the splitting varies as $2p(J+1/2)$ and for $|P|=3/2$ as $2q(J-1/2)(J+1/2)(J+3/2)$.[37] Table IV shows the parity doubling parameters. The energy ordering of the e/f parity states alternates as a function of *J*. The *P*-type doubling is similar to λ-doubling or Ω-doubling in diatomic molecules. The splitting decreases fast with increasing $|P|$ and increases with increasing *J*. For some $|P|=1/2$ states, the parity doubling constants are comparable to the rotational constants. In such cases the parity doubling can have a substantial effect on the level pattern. As mentioned above, the parity splitting for the $n=1$, $|P|=1/2$ and $n=3$, $|P|=3/2$ are affected by a perturbation. Thus, no reliable *q* parameter for the $n=3$, $|P|=3/2$ can be determined.

The existing He droplet spectra of Br–HF[18] are for $|P|=3/2$ states, where the *P*-type doubling is likely to be unresolved. However, it would be very interesting indeed to

TABLE IV. Energy levels (above) and spectroscopic parameters (below) from close-coupling calculations for Br–HF. All quantities are given in cm^{-1}, with energy levels relative to the energy of $Br(^2P_{3/2})+HF(j=0)$. States marked with (*) are affected by a perturbation and are not taken into account to derive spectroscopic parameters from. Derived spectroscopic parameters (in cm^{-1}). Note that more significant figures than are given for the eigenvalues were used in the fits to obtain these values. (*) For $n=3$, $|P|=3/2$ no reliable splitting parameter q could be calculated (see text).

n	Parity	$\|P\|$	$J=1/2$	$J=3/2$	$J=5/2$	$J=7/2$
0	e	1/2	−290.483	−290.256	−289.851	−292.270
0	f	1/2	−290.409	−290.107	−289.628	−288.972
1	e	1/2	−224.642	−224.434	−223.798	−223.510*
1	f	1/2	−224.549	−224.249	−223.057	−223.127*
0,1	e	1/2	−198.153	−198.053	−197.767	−197.296
0,1	f	1/2	−197.804	−197.356	−196.727	−195.916
0,1	e	1/2	−190.059	−189.821	−189.395	−189.784
0,1	f	1/2	−189.980	−189.662	−189.159	−188.471
0	e/f	3/2		−435.295	−434.856	−434.241
1	e/f	3/2		−353.113	−352.692	−352.106
2	e/f	3/2		−282.860	−282.486	−281.927
3	f	3/2		−224.155	−223.758	−223.219*
3	e	3/2		−224.144	−223.756	−223.254*
0	e/f	5/2			−262.635	−262.018
1	e/f	5/2			−195.075	−194.453

n	$\|P\|$	$E-E_0$	B	p	q
0	1/2	144.937	0.0883	0.037	
1	1/2	210.789	0.0855	0.044	
0,1	1/2	237.402	0.0915	0.173	
0,1	1/2	245.361	0.0928	0.040	
0	3/2		0.0879		$<10^{-7}$
1	3/2	82.188	0.0839		$<10^{-7}$
2	3/2	152.421	0.0799		$<10^{-7}$
3	3/2	211.160	0.0785		*

observe an excited state with $|P|=1/2$ and to find out whether the P-type doubling is reduced in a He droplet by a factor similar to the rotational constants.

IV. CONCLUSIONS

We have presented model potential energy surfaces for the Br–HF complex, which has recently been observed in liquid helium droplets.[18] Our potential surfaces are valid at van der Waals distances where the HF molecule retains its identity in the complex. There are three surfaces that correlate with $Br(^2P)$, which can be described in either diabatic or adiabatic and either spin-free or spin-containing representations. All three surfaces, and the couplings between them, are needed for an adequate treatment of the spectroscopy and dynamics.

The Br–HF complex is much more strongly bound than the symmetric complexes Br–HBr, Cl–HCl, and F–HF that have been studied previously. This is because the binding is dominated by the electrostatic interaction between the atomic quadrupole moment on Br and the molecular dipole and quadrupole moments on HF:Br has a larger quadrupole moment than F or Cl, and HF has a larger dipole moment and can approach closer than HCl or HBr.

The most physically realistic representation for visualising the bound states is the adiabatic representation including spin–orbit coupling. For this, our lowest surface has a linear equilibrium geometry, Br–H–F, with a well depth of 670 cm^{-1}. The lowest bound state has a binding energy of 435 cm^{-1}, with excited bending states 145 and 173 cm^{-1} above it. These are the most likely intermolecular vibrations to be observable, either directly in the far infrared or in combination with the HF stretch. We hope that the present work will stimulate efforts to observe infrared combination bands in helium droplet spectra and will encourage further work to observe spectra of these fascinating species in unsolvated form.

ACKNOWLEDGMENTS

The authors are very grateful to Jochen Kupper and Roger Miller for communicating their spectra of Br–HF in helium droplets in advance of publication. M.M. acknowledges partial financial support from the Schweizerischer Nationalfonds through a Förderungsprofessur for work done in Basel.

[1] M.-L. Dubernet and J. M. Hutson, J. Chem. Phys. **101**, 1939 (1994).
[2] M.-L. Dubernet and J. M. Hutson, J. Phys. Chem. **98**, 5844 (1994).
[3] J. M. Hutson, J. Phys. Chem. **96**, 4237 (1992).
[4] M. Meuwly and J. M. Hutson, J. Chem. Phys. **112**, 592 (2000).
[5] M. Meuwly and J. M. Hutson, Phys. Chem. Chem. Phys. **2**, 441 (2000).
[6] C. S. Maierle, G. C. Schatz, M. S. Gordon, P. McCabe, and J. N. L. Connor, J. Chem. Soc., Faraday Trans. **93**, 709 (1997).
[7] A. J. Dobbyn, J. N. L. Connor, N. A. Besley, P. J. Knowles, and G. C. Schatz, Phys. Chem. Chem. Phys. **1**, 957 (1999).
[8] G. C. Schatz, P. McCabe, and J. N. L. Connor, Faraday Discuss. Chem. Soc. **110**, 139 (1998).
[9] T. W. J. Whiteley, A. J. Dobbyn, J. N. L. Connor, and G. C. Schatz, Phys. Chem. Chem. Phys. **2**, 557 (2000).
[10] T. Xie, D. Y. Wang, J. M. Bowman, and D. E. Manolopoulos, J. Chem. Phys. **116**, 7461 (2002).
[11] D. Skouteris, D. E. Manolopoulos, W. S. Bian, H.-J. Werner, L. H. Lai, and K. P. Liu, Science **286**, 1713 (1999).
[12] J. Kłos, G. Chalasinski, M. M. Szczesniak, and H.-J. Werner, J. Chem. Phys. **115**, 3085 (2001).
[13] P. Zdǎnska, D. Nachtigallova, P. Nachtigall, and P. Jungwirth, J. Chem. Phys. **115**, 5974 (2001).
[14] J. Zhang, M. Dulligan, J. Segall, Y. Wen, and C. Wittig, J. Phys. Chem. **99**, 13680 (1995).
[15] K. Liu, A. Kolessov, J. W. Partin, I. Bezel, and C. Wittig, Chem. Phys. Lett. **299**, 374 (1999).
[16] K. Imura, H. Ohoyama, R. Naaman, D. C. Che, M. Hashinokuchi, and T. Kasai, J. Mol. Spectrosc. **552**, 137 (2000).
[17] D.-C. Che, M. Hashinokuchi, Y. Shimizu, H. Ohoyama, and T. Kasai, Phys. Chem. Chem. Phys. **3**, 4979 (2001).
[18] J. Kupper and R. E. Miller (private communication).
[19] J. M. Hutson and B. J. Howard, Mol. Phys. **45**, 791 (1982).
[20] M. Meuwly and J. M. Hutson, J. Chem. Phys. **110**, 8338 (1999).
[21] V. Aquilanti, R. Candori, D. Cappelletti, E. Luzzatti, and F. Pirani, Chem. Phys. **145**, 293 (1990).
[22] V. Aquilanti, D. Cappelletti, V. Lorent, E. Luzzatti, and F. Pirani, J. Phys. Chem. **97**, 2063 (1993).
[23] M. Medved, P. W. Fowler, and J. M. Hutson, Mol. Phys. **98**, 453 (2000).
[24] D. A. Barrow, M. J. Slaman, and R. A. Aziz, J. Chem. Phys. **91**, 6348 (1989).
[25] T. H. Dunning, Jr., J. Chem. Phys. **90**, 1007 (1989).
[26] D. E. Woon and T. H. Dunning, Jr., J. Chem. Phys. **98**, 1358 (1993).
[27] MOLPRO is a package of *ab initio* programs written by H.-J. Werner, with contributions from R. D. Amos, P. J. Knowles, A. Bernhardsson *et al.*, MOLPRO, Version 2000, University of Birmingham, Birmingham, 2000.
[28] S. F. Boys and F. Bernardi, Mol. Phys. **19**, 553 (1970).
[29] K. T. Tang, Phys. Rev. **177**, 108 (1969).

[30] A. D. Buckingham, P. W. Fowler, and J. M. Hutson, Chem. Rev. **88**, 963 (1988).
[31] J. Kłos, G. Chalasinski, R. V. Krems, A. A. Buchachenko, V. Aquilanti, F. Pirani, and D. Capelletti, J. Chem. Phys. **116**, 9269 (2002).
[32] M. Meuwly and J. M. Hutson, J. Chem. Phys. **110**, 8338 (1999).
[33] J. M. Hutson, BOUND computer program, version 5, distributed by Collaborative Computational Project No. 6 of the UK Engineering and Physical Sciences Research Council, 1993.
[34] B. R. Johnson, J. Comput. Phys. **13**, 445 (1973).
[35] J. M. Hutson, Comput. Phys. Commun. **84**, 1 (1994).
[36] R. E. Miller, Faraday Discuss. Chem. Soc. **118**, 1 (2001).
[37] W. H. Green and M. I. Lester, J. Chem. Phys. **96**, 2573 (1992).